Design and Experimental Validation of a Multifunction Single Layer UHF-RFID Tag Antenna

Mohamed EL Bakkali[1], Mohammed Ali Ennasar[1], Otman El Mrabet[1], Raúl Fernández García[2]

[1]Information and Telecommunication Systems Laboratory (LaSiT), FS, Abdelmalek Essaadi University, Tetouan, Morocco
[2]Department of Electronic Engineering, Universitat Politècnica de Catalunya, Terrassa, Spain

Corresponding author: M. El Bakkali (e-mail: elbakkali.mohamed-etu@uae.ac.ma)

ABSTRACT In this paper, we report a new design of a multifunction RFID tag antenna operating in the European band (865-868.5MHz) and the North American band (902-928 MHz) separately. The multifunction behavior can be achieved by changing the position of the RFID chip. It is found that at each feeding position, the RFID tag antenna can operate separately on both bands. The characteristics of the proposed design including S-parameters, impedance and reading range pattern have been investigated using simulation software CST Microwave Studio and experimental results. Further insight into the mechanism radiation is sought through the investigation of the current density and the equivalent circuit model. The tolerance of this design on various background materials is also investigated experimentally. The measured and simulated results show good agreement, providing a simple and low-cost design.

INDEX TERMS RFID tag antenna, Multifunction, Reading range.

I. INTRODUCTION

RADIO frequency identification in collaboration with the Internet of things (IoT) is a rapidly developing wireless technology that uses electromagnetic waves to automatically track various objects: Documents, animals, people and so on [1–6]. This situation has led to great demand in particular for ultra-high frequency UHF-RFID system that can operate throughout the world in different bands such as 865-868 MHz in Europe and North Africa, 866-869 MHz and 923-925 MHz in Singapore, 918-926 MHz in Australia, 902-928 MHz in north and South America, 840.5-844.5 MHz and 920-924.5 MHz in China, 908.5-914 MHz and 950-956 MHz in Korea and Japan. From these licensed spectra for UHF RFID applications, one can conclude that most countries have adopted to use European and north American bands. This situation has triggered research on the design of compact and dual band UHF-RFID tag antennas with simple configurations and easy and fast fabrication process. Some of research works have been conducted on wideband RFID tags [7–10]. However, it is found difficult to achieve a reasonable read range at both frequency bands simultaneously. Up to now, different types of RFID tag antennas are proposed to operate in the European and North American bands [11–13]. For example, in [11] the authors proposed a new dual band RFID tag antenna by using a dual band matching technique to achieve conjugate matching between the chip and the antenna at two very closely frequencies. However, the introduction of this technique inevitably increases the physical size of the antenna to create the dual band characteristics. D. Kim et al. [13] presented a dual band passive RFID tag antenna. The dual band operation is achieved by using an artificial magnetic reflector (AMC) ground plane which can increase the cost of the fabrication. Another issue with this technique is that it has been primarily developed for working in a recessed cavity in metallic objects. Printing RFID tag antennas on flexible substrate [12–16] has become a prominent research field within the last decade owing to the demand for wearable health monitoring devices, environmental monitoring, smart packaging, internet of things (IoT), medical applications, and vehicular technology. The main focus of these papers was to extend the scope of the RFID technology to sensing applications where the reading range is not a critical parameter. In this paper, we look into alternative approach to develop a multifunction RFID tag antenna that work on two different bands separately. This feature can be reached by changing the position of the RFID chip. At each feeding position, the RFID tag antenna can operate separately at European and north American bands without enlarging the RFID tag antenna size. This technique leads to an easy and simple matching and fabrication process without increasing the whole size of the tag. Furthermore, the reading range for European and American bands is closely similar. These features cannot be achieved simultaneously when designing dual band RFID tag antennas. The mechanism of multifunction behavior can be easily realized by etching four novel unequal rectangular patches at the vertexes of the rectangular radiator. The pro-

posed structure shows some distinct features. It is simple in fabrication and not requiring complex matching elements to operate on two different bands, separately.

II. MULTIFUNCTION RFID TAG ANTENNA CONFIGURATION AND DESIGN ANALYSIS

A. TAG ANTENNA DESIGN

The configuration of the proposed multifunction RFID tag antenna is shown in Fig. 1. This RFID tag antenna is a single layer metallic structure and can easily printed on a cheap substrate. In this study, the RFID tag antenna is etched on the top surface of the FR-4 substrate material which have a thickness of 1.6 mm, relative permittivity of 4.4 and a loss tangent of 0.02. The whole antenna size is 102 mm$\times$64 mm$\times$1.6 mm which corresponds to $0.268\lambda_0$ $\times 0.097\lambda_0$ $\times 0.004\lambda_0$, where λ_0 is the free-space wavelength at 915 MHz. The physical structure of this proposed design consists of a rectangular loop with a small gap on each of two longer sides. To get a good impedance matching at both European and American bands separately, four rectangular patches are positioned along the diagonal lines at the four vertexes as shown in Fig. 1. The RFID chip used in this design is Murata (LXMS31ACNA) chip [17], with an equivalent resistance of 17.6 Ω and a capacitance of 1.62 pF in series at 915 MHz, and has a minimum power activation of -8 dBm.

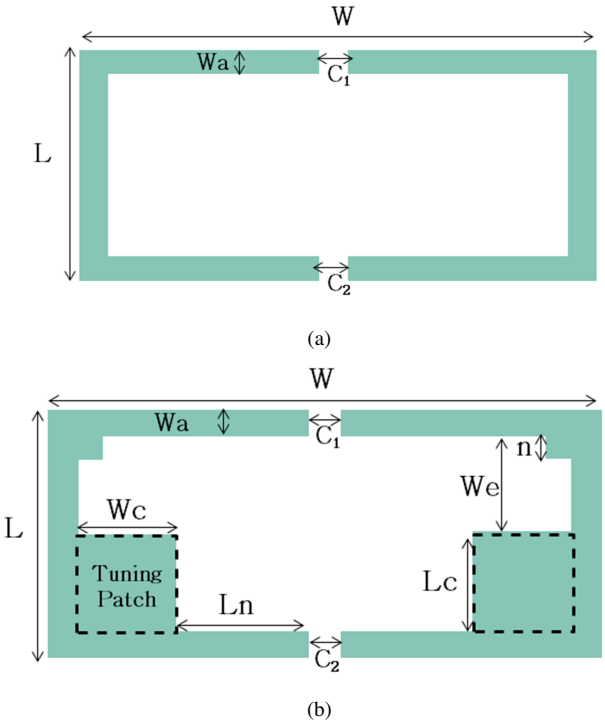

FIGURE 1: Configuration of the RFID tag antenna a) before adding parasitic elements b) last prototypes.

The RFID chip used in this work exhibits a high capacitive measured reactance Z_{chip} = 17.2-j100.9 Ω [18], which can be cancelled by adding rectangular patch at each corner of the loop. This technique provides an easy input impedance matching. Furthermore, by properly chosen the dimensions of Lc and Wc, this technique allows the tuning of the operating frequency of the proposed structure to operate in the US and European bands, separately, depending on the RFID chip position (C_1 or C_2), as shown in Fig. 1b. Referring to Fig. 1b, the final optimized geometrical parameters of the proposed design obtained by using CST Microwave studio are listed in Table. 1.

TABLE 1: The optimized parameters value of the studied RFID tag antenna in millimeter (mm).

Parameter	Dimension
W	78
L	22
We	5
Ln	21
Wc	11
Lc	13
Wa	3
n	1.8
C1	2
C2	2

B. TAG ANTENNA DESIGN ANALYSIS

The design procedure of the proposed RFID tag antenna is now discussed. It starts with a simple rectangular loop antenna with a small gap on each of two longer sides (Fig. 1a). The rectangular loop antenna structure is symmetrical for both axes so the results are identical no matter where the RFID chip is placed in positions C_1 (named as Ant1) or in C_2 (named as Ant2). Fig. 2 shows that the input impedance of the first design at 868 MHz and 915 MHz is approximately 14+j120 Ω, and 20+j230 Ω, respectively. At 868 MHz, the reactive part of the input impedance is close to the one of the RFID IC chip. Even though, it needs to be a little bit further adjusted. In contrast, the antenna achieves a high reactance at 915 MHz which has caused it to be poorly matched with the complex conjugate of chip's impedance.

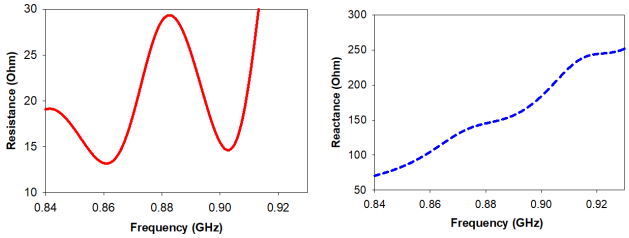

FIGURE 2: Simulated input impedance of the first proposed RFID tag antenna.

Hereafter, four tuning patches are introduced into the initial design of the antenna structure at the four vertexes as shown in Fig. 1 for improving the impedance matching and the power transmission coefficient, especially at the North American band. Two of the rectangular patches with size $L_c \times W_c$ are placed at the lower vertexes, whereas the two square patches with size n$\times$n are placed at the upper vertexes.

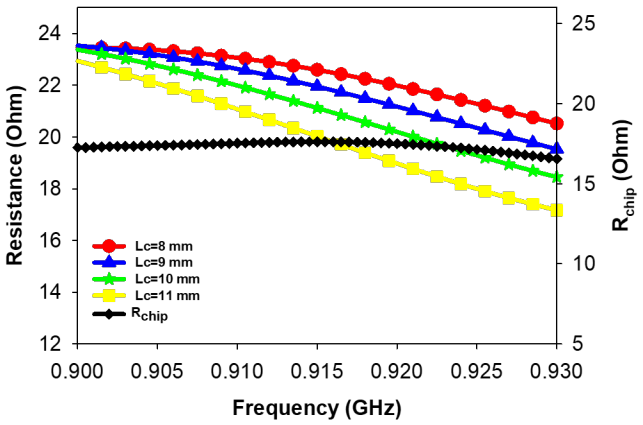

(a)

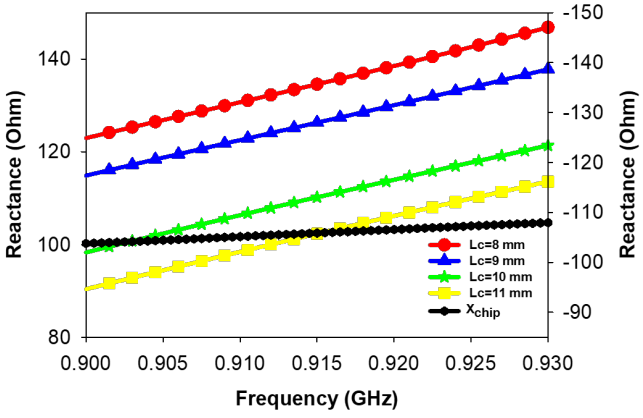

(b)

FIGURE 3: Simulated input impedance of the proposed RFID tag antenna for different length LC of the tuning patch at the North American band.

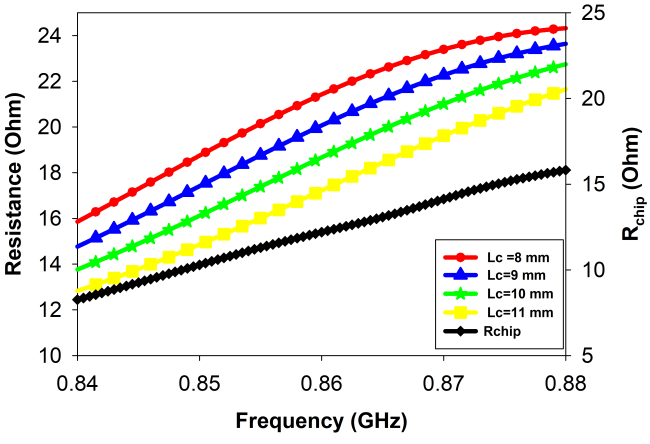

(a)

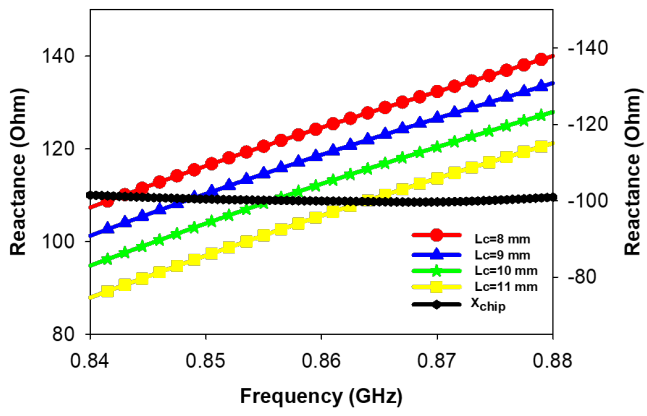

(b)

FIGURE 4: Simulated input impedance of the proposed RFID tag antenna for different length LC of the tuning patch at the European band.

It should be noted that, first we have introduced the two small patches located at the upper vertexes to change a little bit the input impedance of the Ant1 so that we can have a good impedance matching. Then, we have introduced the bigger patches which allow us to improve both the power transmission coefficient and the impedance matching at both North American and European bands. Thus, the effect of varying the values of L_c on the resistance and reactance of the proposed RFID tag for Ant2 is studied, and the results are presented in Fig. 3 and Fig. 4, respectively. As we can see in Figs.3 and 4, shortening Lc causes the RFID tag resistance and the reactance to increase, allowing the tag resonant frequency to be tuned easily. The RFID tag becomes more inductive with decreasing L_c.

After presenting the design steps and the parametric study given above, the corresponding surface current density analysis of both configurations (Ant1 and Ant2) is explored here. Fig. 5 shows that the current path of the Ant1 is longer than the one of the Ant2, which lead to a raising of the Ant1 inductance and resulting in a lower resonant frequency.

An equivalent circuit model has been developed as shown in Fig. 6 for analyzing the input impedance characteristics to further get physical insight into the antenna resonance. For the sake of simplicity, the RFID chip and the antenna are modelled as a series RC (R_{chip}, C_{chip}) and a series RLC circuit (R_{ant}, L_{ant}, C_{ant}), respectively.

The approximate values of the antenna elements R_{ant}, and L_{ant} were computed using (1) [16] and (2) [20], respectively. Noting that μ_0=4π×10^{-7} H/m.

$$L_{ant,M} = \frac{\mu_0}{2\pi} l(\ln(\frac{L}{W})) + \frac{\pi}{2} \tag{1}$$

$$R_{ant} = 80\pi^2\alpha^2(\frac{L}{\lambda})^2 \tag{2}$$

Where the factor (α) in (2) was approximated by using (3) [21]. The equation (1) depends only on the length of the dipole (l) and the wavelength.

$$\alpha = \frac{1-\cos\frac{\pi L}{\lambda}}{\frac{\pi L}{\lambda}\sin\frac{\pi L}{\lambda}} \tag{3}$$

The capacitance (C_{ant}) of the antenna can obtained by using the resonance frequency equation:

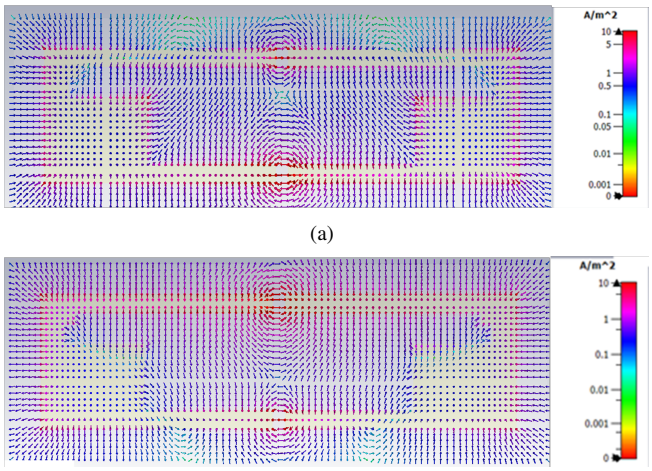

(a)

(b)

FIGURE 5: Surface current distributions. (a) Ant1 at 868 MHz, (b) ant2 at 915 MHz.

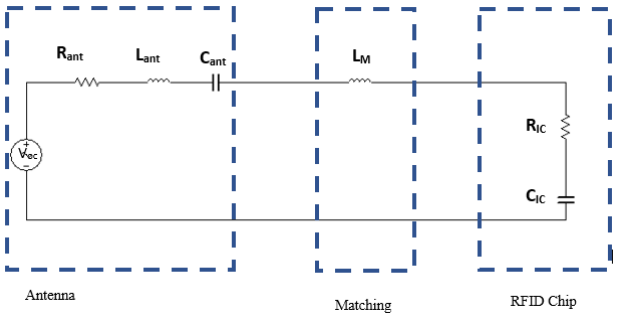

FIGURE 6: Equivalent circuit for the presented RFID tag antenna.

$$f = \frac{1}{2\pi\sqrt{L_a \times C_a}} \tag{4}$$

The inductance (L_M) can be calculated in the same manner as explained in the case of (L_{ant}). It worth to mention that some components were tuned using ADS software to be close to the full wave simulation results.

III. RESULTS AND DISCUSSION

In this section, the simulated structure is fabricated using LPKF Protomat S100 available in our laboratory to verify the predicted results presented above. This machine (See Fig. 7a) has a resolution of 0.01 mils (0.25 µm) and a maximum milling speed of 6 inch/s. It is also an ideal system for rapid and low-cost fabrication. The fabricated protype is shown in the inset of Figure 7(a). The reflection coefficient and input impedance of the proposed designed is measured using a N5234B PNA-L Microwave Network Analyzer through a differential probe as shown in Fig. 7(b).

The measured results of the reflection coefficient for both configurations as a function of the frequency are compared

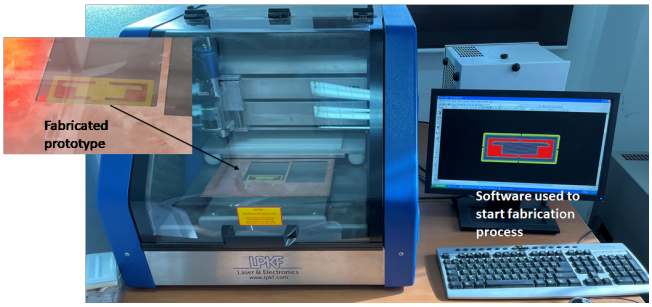

(a)

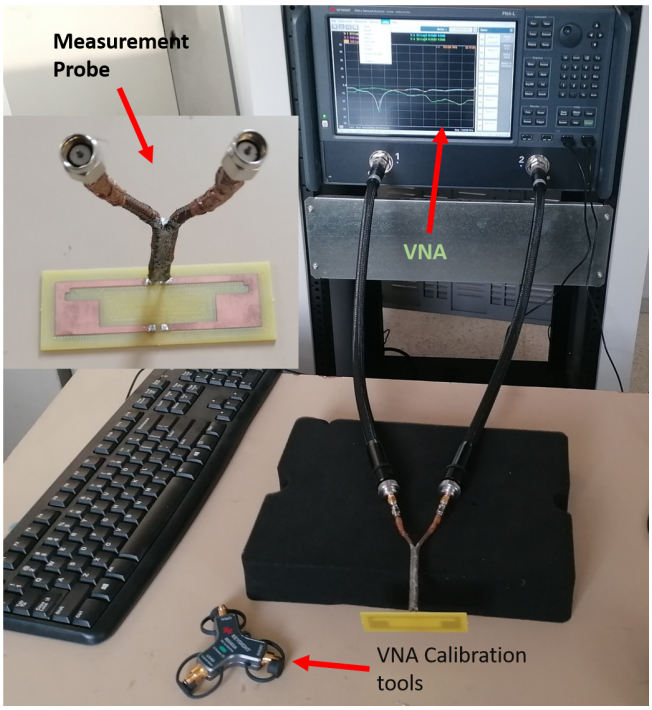

(b)

FIGURE 7: (a) Fabricated prototype, (b) experimental set-up form measuring the impedance of the fabricated structure.

with the simulated and modeled ones in Fig. 8(a) and 8(b). We can see a good agreement between all data sets. Only small average differences were noticed between measured and full wave simulation on the one hand and the equivalent circuit model on the other hand. This can be attributed to the use of the approximated equations to calculate all the lumped elements, and even so, the proposed circuit model can accurately predict the reflection coefficient. For Ant1, the measured -10 dB bandwidth is ranging from 900 MHz to 928 MHz for a total bandwidth of 28 MHz and is centered at 914 MHz, which can cover totally the North-American UHF-RFID band. Whereas, for Ant2, the measured -10 dB bandwidth is ranging from 865 MHz to 868 MHz for a total bandwidth of 10 MHz and is centered at 867 MHz, which can cover totally the European UHF-RFID band. Fig.9 shows the measured and simulated input impedance for both configurations in free space. It worth mentioning that these

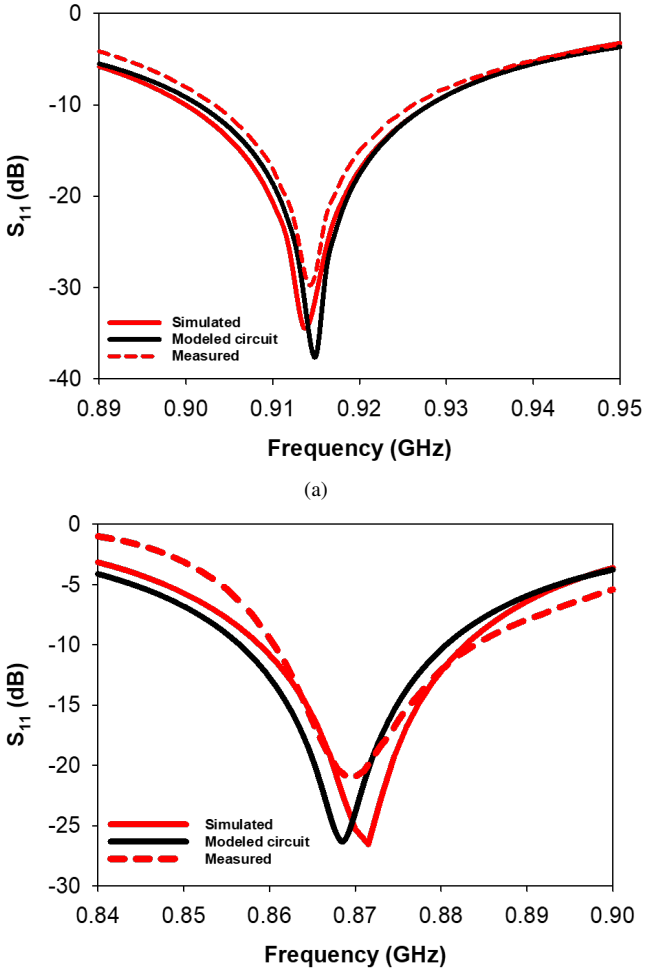

FIGURE 8: Simulated and measured reflection coefficients: (a) for 915 MHz, (b) for 868 MHz

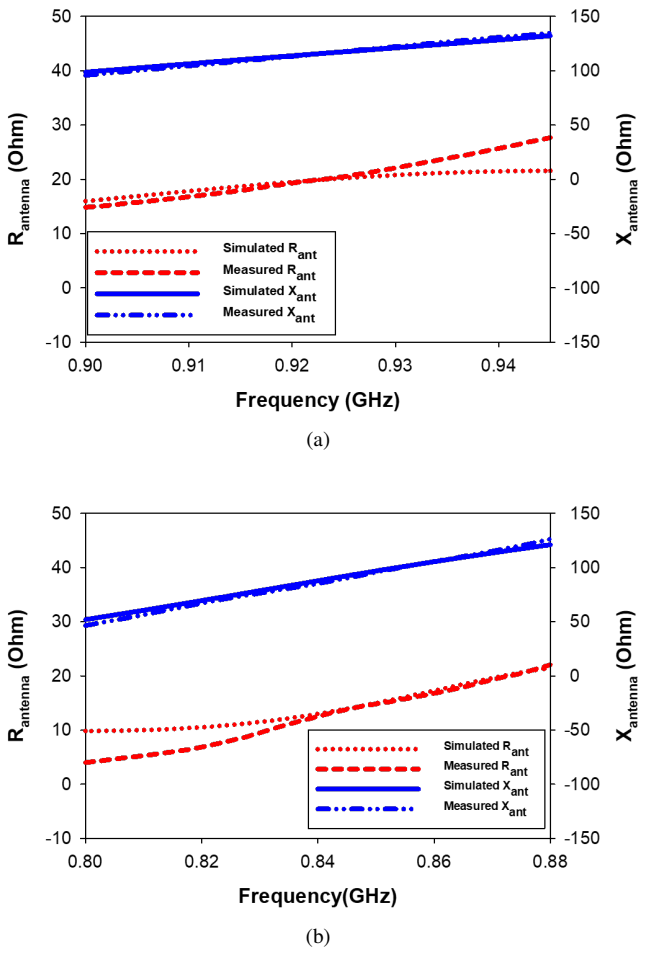

FIGURE 9: Simulated and measured antenna impedance: (a) for 915 MHz, (b) for 868 MHz

results are obtained using the same method described in [18]. The RFID tag antenna's input impedance is calculated by the measured S-parameters given above and using the above equation from [22].

$$Z_d = \frac{2Z_0(1 - S_{11}^2 + S_{21}^2 - 2S_{12}^2)}{(1 - S_{11})^2 - S_{21}^2} \tag{5}$$

Where Z_0 is the coaxial cable's characteristic impedance. From measurement, the impedance of the Ant1 is approximately 17.9+j110 Ω which is very close to the simulated one 18.7+j108.8Ω at 915MHz. However, for Ant2 the measured input impedance is 18.8+j112.3Ω while the simulated one is 19.43+j112.3Ω at 868 MHz. These results are good enough to guarantee a maximum power transfer between the RFID chip for both configurations. A small discrepancy can be observed between the measured and simulated results (input impedance), which may be attributed to the soldered measurement probe (See Fig. 7).

Subsequently, we measured the reading range in free space, which is the most vital parameter that determines the performance of an RFID tag antenna. This can be obtained by using the Friis free-space Formula [23]:

$$r = \frac{\lambda_0}{4\pi}\sqrt{\frac{P_r G_r G_{tag} \tau}{P_{th}}} \tag{6}$$

Where λ_0 is the free space wavelength, P_r = 1 W is the power transmitted by the reader, G_r = 6 dBi is the gain of the reader antenna, G_{tag} is the gain of the RFID tag antenna, and τ is the power transmission coefficient. Besides, P_{th} = -8 dBm (LXMS31ACNA IC chip) is the minimum power threshold needed to provide enough power to the chip (sensitivity). The measurement setup used in this work to measure the reading range of both configurations has been deployed in an ordinary room (see Fig. 10). It should be noted that this measurement setup is similar to the one reported in [24]. It consists of a Thing Magic Micro (M6e-M) reader [25] connected to a single circularly polarized patch antenna with a gain of 6 dBi in the frequency band between 0.8 GHz and 1GHz. The RFID reader is connected to the circularly polarized antenna through 1.8 m of 50 Ω coaxial cable (model CNT-195-FR) to generate 30 dBm at 915 MHz. Hence,

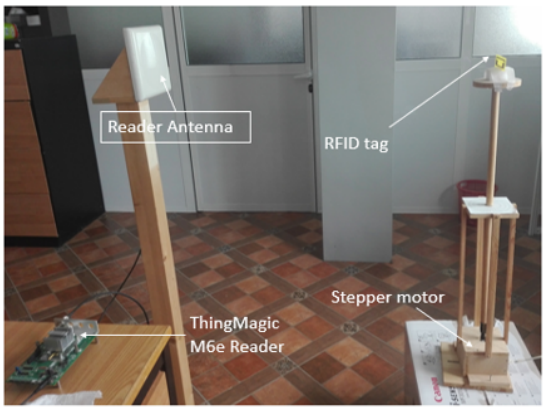

FIGURE 10: Read range measurement setup.

the total transmitted power is approximately 4W which is the maximum value of EIRP (effective isotropic radiated power) allowed by the federal communications commission (FCC) at 915 MHz. The whole system is controlled by a homemade software installed in a computer to plot in real time the measured activation power and reading range. The distance between the polarized patch antenna and the RFID tag antenna in this setup, which are aligned in parallel, is 1 meter to meet far field requirement.

Fig. 11 shows the measured and simulated reading range of both configurations (Ant1 and Ant2). It is observed that the measured reading range for Ant1 at 868 MHz is near to 5 meters and for Ant2 at 915 MHz is 4 meters.

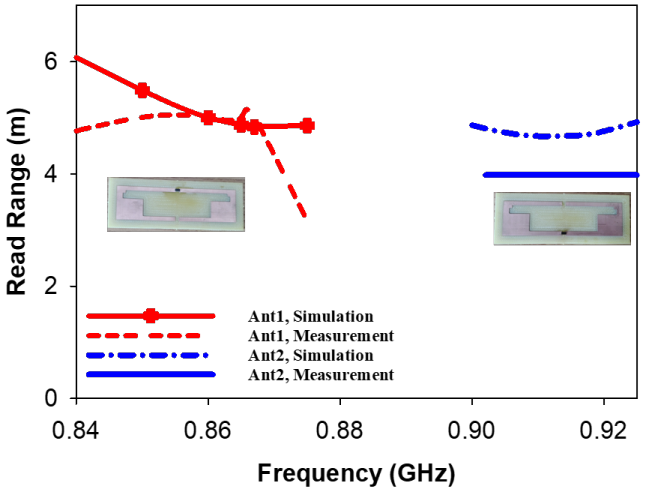

FIGURE 11: Measured and simulated read range for both configurations

It is worth mentioning that the proposed design can demonstrate at both bands higher reading range, for the reason that the RFID chip used in this work has a minimum power required to activate the chip P_{th} = - 8 dBm, and this value is certainly lower than the half of the other RFID chips such as NXP-G2XL and Alien-Higgs 4. For instance, if an Alien-Higgs 4- IC chip with P_{th} = -20.5 dBm [26] was

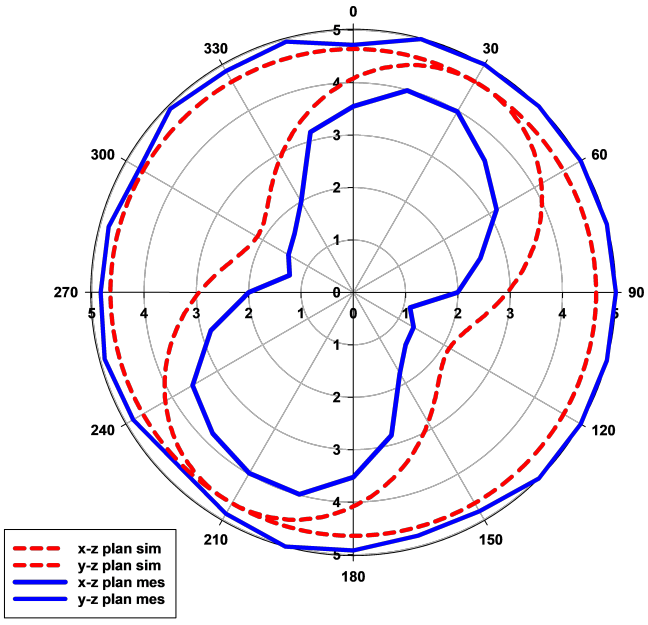

(a)

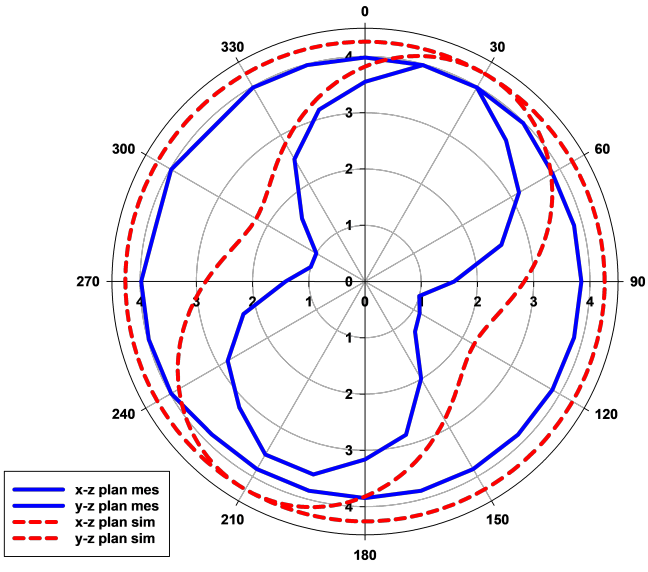

(b)

FIGURE 12: Measured read range patterns in *x-y* and *y-z* planes: (a) for Ant1(868 MHz), (b) for Ant2(915 MHz)

used in the presented design, the calculated reading range would be approximately 19 meter. Even though, the obtained reading range is better than one design published in [24].

The measured and simulated reading range patterns in *x-z* and *y-z* planes are investigated and plotted in Fig. 12.

Fig. 12 shows that Ant1 and Ant2 have a fairly good omnidirectional read pattern in the *x-y* plane. Besides that, it can see clearly that in the *x-z* plane, Ant1 and Ant2 have a maximum reading range of about 4 m obtained at the angle of ϕ=310° and ϕ=210°, respectively. This implies that the both configurations (Ant1 and Ant2) and the RFID

FIGURE 13: Read range measurement on different objects.

TABLE 2: Measured reading range for different materials (m).

Materials (Thickness)	Free space	Plastic (0.7 mm)	Carton (2 mm)	Wood (7 mm)	Metal (7 mm)
Frequency					
915 MHz	4	4	3.56	2	0.45
867 MHz	4.5	4	2.8	1.57	0.35

reader antenna have the same polarization at these particular angles. Furthermore, it is worthwhile to mention that the maximum value of the read range is different in both planes *x-y* and *y-z* owing to uncertainties in positioning the RFID tag antenna with respect to the reader in both planes. So far, the performances of the proposed RFID tag antenna were characterized in free space, its performances on different substrate including metallic object are also investigated, as shown in Fig. 13. The obtained results are summarized in Table 2. It can be observed that the reading range of the proposed RFID tag antenna decreases drastically when mounted on metallic plate. This can be ascribed to the out of image current density created above the metallic plate which leads to a drastic reduction of the characteristics of the RFID tag in terms of impedance mismatch. To gain further insights on the degradation of the reading range of the proposed design when mounted on different substrates (Plastic, Carton and Wood), we have calculated the reflection coefficient as a function of frequency for each case using CST Microwave studio. The obtained results are plotted in Figure 14.

We can clearly see that the reflection coefficient dependent on the characteristic of the surrounding substrate, any change in terms of the permittivity in the latter will affect the matching between the antenna and the RFID chip, hence

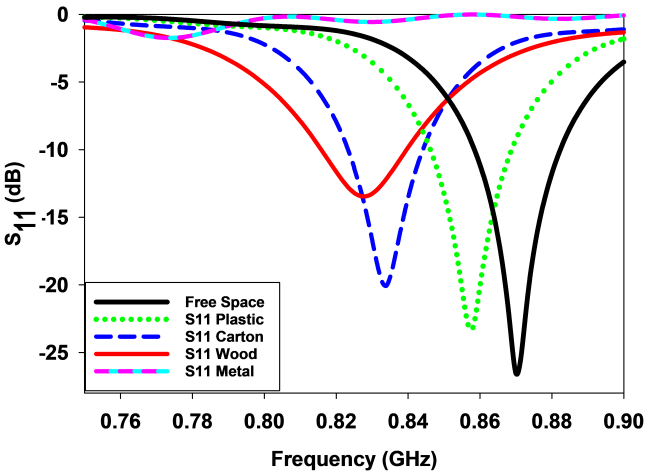

(a)

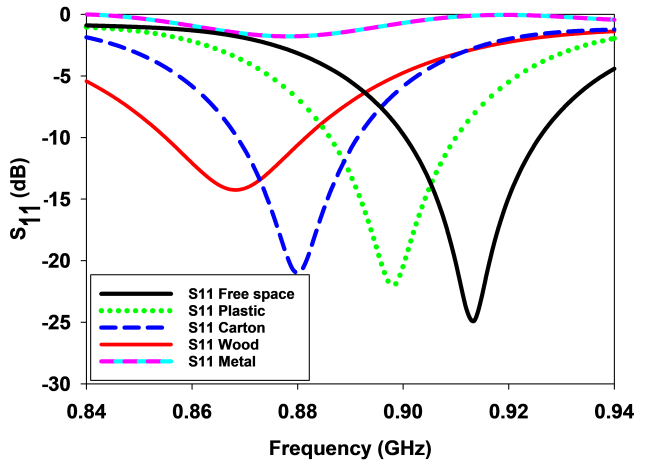

(b)

FIGURE 14: Simulated reflection coefficients of both configurations (Ant1 and Ant2) mounted on different substrates: (a) Ant1 and (b) ant2.

the reading range. Figure 14 also reveals that the matching between the antenna and the chip decreases increasingly when the tag is mounted on plastic, carton wood and metal, respectively. That's explain the results in terms of the read range presented in Table 2.

IV. CONCLUSION

This paper presents a new multifunction RFID tag antenna that can operates in two different bands by changing the position of the RFID chip. The measured reading range in free space for both configurations is 4 meters (European band) and 5 meters North American band). The proposed RFID tag antenna has also been tested on different substrate (Wood, plastic, and Carton) and on a metallic plate. Measurements show that the reading range is very sensitive to the variation of the objects on which the RFID tag is mounted, which makes it suitable for sensing applications, in particular for

the determination of the concentration of aqueous solutions. The measured and simulated results show good agreement, providing a simple, multifunction and low-cost design.

REFERENCES

[1] L. Ukkonen, M. Schaffrath, D. W. Engels, L. Sydänheimo, and M. Kivikoski, ''Operability of folded microstrip patch-type tag antenna in the UHF RFID bands within 865-928 MHz," IEEE Antennas Wirel. Propag. Lett., vol. 5, no. 1, pp. 414–417, 2006.

[2] P. Muianga,'' RFID Handbook: Fundamentals and Applications in Contactless Smart Cards, Radio Frequency Identification and Near-Field Communication, Third Edition." .

[3] D. M. Dobkin, The RF in RFID: UHF RFID in Practice: Second Edition. Elsevier Inc., 2012.

[4] H. Li, J. Zhu, and Y. Yu, ''Compact Single-Layer RFID Tag Antenna Tolerant to Background Materials,"IEEE Access, vol. 5, pp. 21070–21079, 2017.

[5] M. A. Ennasar, O. El Mrabet, K. Mohamed, and M. Essaaidi, ''Design and characterization of a broadband flexible polyimide RFID tag sensor for NaCl and sugar detection,"Prog. Electromagn. Res. C, vol. 94, no. August, pp. 273–283, 2019.

[6] A. Hamani, M. C. E. Yagoub, T. P. Vuong, and R. Touhami,''A novel broadband antenna design for UHF RFID tags on metallic surface environments," IEEE Antennas Wirel. Propag. Lett., vol. 16, pp. 91–94, 2017.

[7] L. Xu, B. J. Hu, and J. Wang,''UHF RFID tag antenna with broadband characteristic," Electron. Lett., vol. 44, no. 2, p. 79, 2008.

[8] Z. J. Tang, Y. G. He, and Y. Wang,''Broadband UHF RFID tag antenna with quasi-isotropic radiation performance," AEU - Int. J. Electron. Commun., vol. 65, no. 10, pp. 859–863, Oct. 2011.

[9] F. Paredes, G. Zamora, F. J. Herraiz-Martínez, F. Martín, and J. Bonache, '' Dual-band UHF-RFID tags based on meander-line antennas loaded with spiral resonators," IEEE Antennas Wirel. Propag. Lett., vol. 10, pp. 768–771, 2011.

[10] F. Paredes, G. Z. Gonzlez, J. Bonache, and F. Martin, ''Dual-band impedance matching networks based on split-ring resonators for applications in RF identification (RFID)," IEEE Trans. Microw. Theory Tech., vol 58, no. 5 PART 1, pp. 1159-1166, May 2010.

[11] D. Kim and J. Yeo, ''Dual-band long-range passive RFID tag antenna using an AMC ground plane," IEEE Trans. Antennas Propag., vol. 60, no. 6, pp. 2620–2626, 2012.

[12] M. El Khamlichi, A. A. Melcon, O. El Mrabet, M. A. Ennasar, and J. Hinojosa, " Flexible UHF RFID tag for blood tubes monitoring," Sensors (Switzerland), vol. 19, no. 22, 2019.

[13] M. El Bakkali, O. El Mrabet, M. Kanjaa, I. Gil, and E. Bakkali, ''An Embroidered Passive Textile RFID Tag Based on a T-Matched Antenna," vol. 101, no. September, pp. 137–145, 2021.

[14] Y. Wang et al., ''Flexible RFID Tag Metal Antenna on Paper-Based Substrate by Inkjet Printing Technology," Adv. Funct. Mater., vol. 29, no. 29, p. 1902579, Jul. 2019.

[15] M. T. Islam, T. Alam, I. Yahya, and M. Cho, Flexible Radio-Frequency Identification (RFID) Tag Antenna for Sensor Applications," Sensors 2018, Vol. 18, Page 4212, vol. 18, no. 12, p. 4212, Nov. 2018.

[16] M. Hussain, Y. Amin, and K. G. Lee, ''A Compact and Flexible UHF RFID Tag Antenna for Massive IoT Devices in 5G System," Sensors 2020, Vol. 20, Page 5713, vol. 20, no. 19, p. 5713, Oct. 2020.

[17] G. Descriptions ''MAGICSTRAP Technical Data Sheet Murata part number: LXMS31ACNA -LXMS31ACMD MAGICSTRAP Technical Data Sheet Murata part number: LXMS31ACNA - LXMS31ACMD"2012.

[18] I. Aznabet, M. A. Ennasar, O. El Mrabet, G. Andia Vera, M. Khalladi, and S. Tedjni, ''A broadband modified T-shaped planar dipole antenna for UHF RFID tag applications," Prog. Electromagn. Res. C, vol. 73, no. April, pp. 137–144, 2017.

[19] A. P. Sohrab, Y. Huang, M. Hussein, M. Kod, and P. Carter, ''A UHF RFID tag with improved performance on liquid bottles," IEEE Antennas Wirel. Propag. Lett., vol. 15, no. c, pp. 1673–1676, 2016.

[20] D. D. Deavours, '' Analysis and design of wideband passive UHF RFID tags using a circuit model," 2009 IEEE Int. Conf. RFID, pp. 283–290, 2009.

[21] K. Sockolov, ''UHF RFID ANTENNA IMPEDANCE MATCHING TECHNIQUES," no. March, 2017.

[22] X. Qing, C. K. Goh, and Z. N. Chen, ''Impedance characterization of rfid tag antennas and application in tag co-design," IEEE Trans. Microw. Theory Tech., vol. 57, no. 5, pp. 1268–1274, 2009.

[23] G. Marrocco, E. Di Giampaolo, and R. Aliberti, ''Estimation of UHF RFID reading regions in real environments," IEEE Antennas Propag. Mag., vol. 51, no. 6, pp. 44–57, Dec. 2009.

[24] R. Colella, L. Catarinucci, P. Coppola, and L. Tarricone, ''Measurement Platform for Electromagnetic Characterization and Performance Evaluation of UHF RFID Tags," IEEE Trans. Instrum. Meas., vol. 65, no. 4, pp. 905–914, Apr. 2016.

[25] M. P. Guide and For, Supported Hardware. 2003, pp. 10–13. [Online]. Available : https://www.mouser.com/pdfDocs/TM$_$Micro$_$Micro-LTE-UG-Rev-06292018.pdf.

[26] Alien Technology, ''Higgs 4 SOT," Online, p. 4, 2014. [Online]. Available : http://www.alientechnology.com/wp-content/uploads/Alien-Technology-Higgs-SOT.pdf.